Case-Encapsulated Triboelectric Nanogenerator for Harvesting Energy from Reciprocating Sliding Motion

Qingshen Jing,[†,‡,⊥] Guang Zhu,[†,⊥] Peng Bai,[†] Yannan Xie,[†] Jun Chen,[†] Ray P. S. Han,[‡] and Zhong Lin Wang[†,§,*]

[†]School of Materials Science and Engineering, Georgia Institute of Technology, Atlanta, Georgia 30332-0245, United States, [‡]College of Engineering, Peking University, Beijing 100871, China, and [§]Beijing Institute of Nanoenergy and Nanosystems, Chinese Academy of Sciences, Beijing 100083, China. [⊥]Q. Jing and G. Zhu contributed equally.

ABSTRACT Reciprocating motion is a widely existing form of mechanical motion in natural environment. In this work we reported a case-encapsulated triboelectric nanogenerator (cTENG) based on sliding electrification to convert reciprocating motion into electric energy. Patterned with multiple sets of grating electrodes and lubricated with polytetrafluoroethylene (PTFE) nanoparticles, the cTENG exported an average effective output power of 12.2 mW over 140 kΩ external load at a sliding velocity of 1 m/s, in corresponding to a power density of 1.36 W/m^2. The sliding motion can be induced by direct-applied forces as well as inertia forces, enabling the applicability of the cTENG in addressing ambient vibration motions that feature large amplitude and low frequency. The cTENG was demonstrated to effectively harvest energy from human body motions and wavy water surface, indicating promising prospects of the cTENG in applications such as portable and stand-alone self-powered electronics.

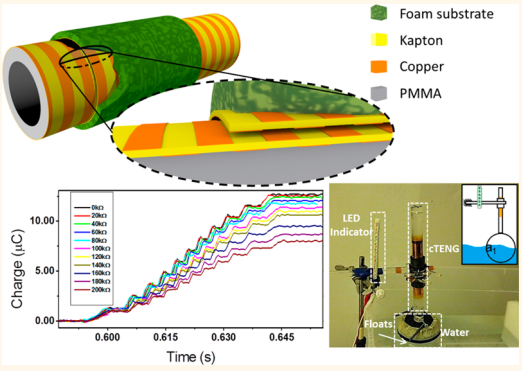

KEYWORDS: reciprocating motion · energy harvesting · triboelectric nanogenerators · casing · self-powered

Harnessing ambient mechanical energy is attracting a lot of attention due to the fast development of portable electronics and sensor networks.[1,2] Mechanisms using piezoelectric,[3−6] electrostatic[7,8] or electromagnetic[9,10] principles to harvest energy from random vibrations,[11] wind flow,[12] air pressure,[13] or human body motions[14] have been developed and applied as generators or self-powered sensors.[13,15] Recently, the development of triboelectric nanogenerators (TENGs) offers a new paradigm for fabricating high-output and cost-effective generators for driving small electronics.[16−19] Reciprocating motion is a very common mechanical motion that occurs in natural oscillations, motion of waves, swing of human limbs, and mechanical piston movements, *etc.* Features of these motions that include long reciprocating distance, low frequencies and amplitude or frequency fluctuations pose challenges for previously developed vibration-harvesters,[11,20−23] which were only suited to low-amplitude and high-frequency excitations induced by inertia forces.

Here we report a compact case-encapsulated triboelectric nanogenerator (cTENG) that targets reciprocating motions driven by either direct or inertia forces. The cTENG relies on electrode pairs that have fine-grating patterns on cylindrical sliding surfaces to generate alternating current. Operating at a sliding velocity of 1 m/s over a sliding distance of 3.8 cm, a cTENG with an effective contact area of 90 cm^2 could generate an output charge of 12.7 μC in a single full slide, which corresponds to an average output DC current of as high as 0.35 mA. At the matched load of 140 kΩ, an average output power of 12.2 mW was achieved. We demonstrated the use of cTENG to harness oscillating motion from sources such as human and water wave motions as an indication of its potential in portable self-powered electronics and power generation.

RESULTS AND DISCUSSION

The structural configuration of the cTENG is depicted in Figure 1 by using two concentric

* Address correspondence to zlwang@gatech.edu.

Received for review February 4, 2014 and accepted March 4, 2014.

Published online March 06, 2014
10.1021/nn500694y

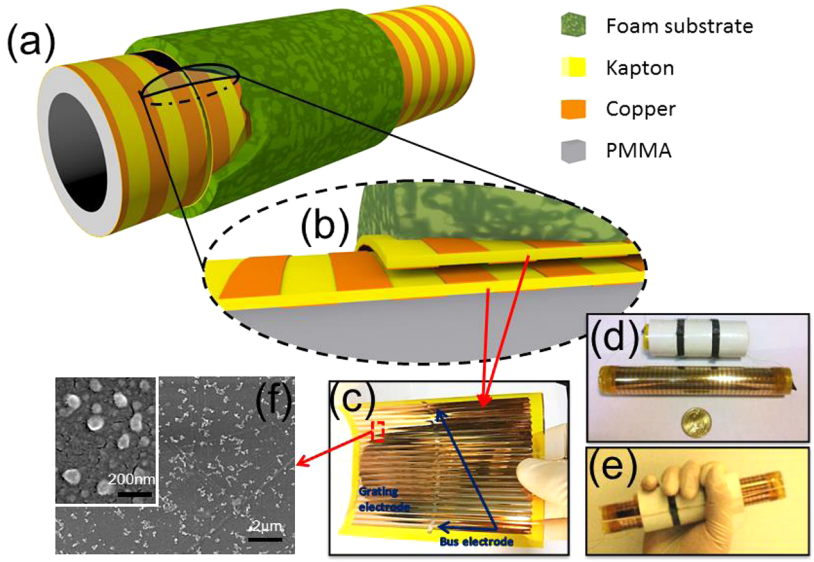

Figure 1. Case-encapsulated triboelectric nanogenerator (cTENG). (a) 3D model of cTENG and (b) cross-section view. (c) Kapton film deposited with grating copper electrode on both sides. A cTENG is shown (d) before and (e) after assembly, with 1 U.S. dollar coin as reference. (f) SEM image with different scales showing PTFE particles spread on the surface of Kapton.

cylinders that can slide one against the other. The basic principle of the cTENG relies on sliding triboelectrification at the interface. The case wrap applied tightly around the outer cylinder allows the two cylindrical structures to move in a coaxial 1-D motion relative to each other. Polyimide film (Kapton) was selected as an electrification material for generating triboelectric charges and also as the supporting substrate. The Kapton film was chosen as it possesses good electrification and tensile strength properties (see S1 from Supporting Information (SI) for details), leading to a high-performance in electricity generation and durability. On both sides of the Kapton film, copper stripes (width of 2 mm) were deposited with a linear pitch of 4 mm. The electrode patterns on different sides exhibited a linear shift of half pitch so that they are complementary to each other (Figure 1b, 1c). Two Kapton films having the same electrode patterns formed a pair of contact surfaces (Figure 1b). All copper stripes on the two contact surfaces were connected by bus electrodes to form a common inner electrode (IE), while those on back surfaces of the Kapton films constituted an outer electrode (OE) (Figure 1c). Spherical polytetrafluoroethylene (PTFE) nanoparticles were spread between the contact surfaces (Figure 1f) as lubricant to reduce friction and to further improve energy conversion efficiency (see details in S2 from SI). The two prepared Kapton films with electrodes were applied on the outer surface of a PMMA tube and the inner surface of a foam tube, respectively (Figure 1d). The fully assembled cTENG is shown in Figure 1e.

The electricity generation mechanism of the cTENG is illustrated in Figure 2. The outer tube slides relative to the inner tube, forming a reciprocating movement. As working mechanism of the cTENG, when Kapton and copper are brought into contact, the difference in triboelectric polarities (see table in S1 from SI) determines that electrons are injected from copper into Kapton (Figure 2a).[19,24,25] The triboelectric charges are equivalent in amount but opposite in polarities. At the state shown in Figure 2a$_1$, all triboelectric charges are balanced, producing no electric field in surrounding space provided that edge effect is ignored. Once sliding motion takes place, the aligned stripes start to mismatch. As a result, negative triboelectric charges on the surface of Kapton films become uncompensated, producing a dipole polarization along the direction of the displacement and thus a potential difference between the IE and the OE. If the two electrodes are electrically connected through an external circuit (Figure 2a, 2a$_{1-5}$), such a potential difference results in a flow of electrons from the OE to the IE, which screens the potential difference induced by the triboelectric charges (Figure 2a$_2$). Consequently, a current from the IE to the OE is simultaneously generated. As the mismatch continues to expand because of sliding, more positive charges are transferred from the IE to the OE until the state shown in Figure 2a$_3$ is reached. Further sliding motion beyond this state leads to a reverse flow of electrons between electrodes, which corresponds to a current with an opposite direction (Figure 2a$_4$). Therefore, a sliding distance for a pitch period can generate a complete cycle of alternating current.

Employing a finite-element method (FEM) technique, a computer simulation of the open-circuit voltage (V_{oc}) as a function of displacement is shown in Figure 2b, 2c (see Methods for detailed simulation description). The largest voltage between the IE and the OE appears when copper stripes on contact surfaces are in

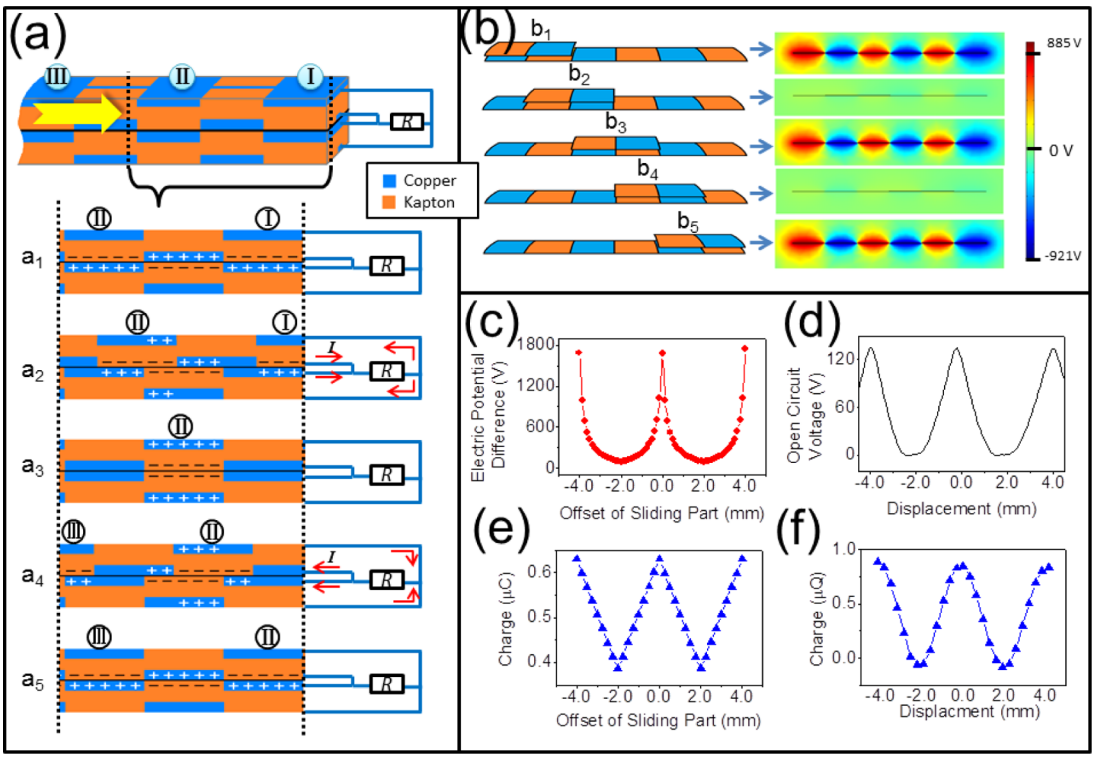

Figure 2. Working mechanism for cTENG and simulation results compared with measurement. (a) Certain area of the cross section is schematically shown, with inner electrodes (IE) and outer electrodes (OE) connected together respectively. Roman numerals are flagged to the electrode stripes to mark relative movement in (a_1)−(a_5). Red arrows indicate the direction of current. (b) Simulation results show a simplified model with 1 unit of stripe sliding over 3 units of stripe. (b_1)−(b_5) show potential distributions induced at critical positions. (c) Simulation results show electric potential difference between the IE and the OE during sliding under open circuit condition. (d) Measured electric potential difference between the IE and the OE over displacement under open circuit condition. (e) Simulation results show charge from one electrode transferred out and in during sliding under short circuit condition. (f) Partial charge curve integrated from measured current data.

complete alignment (Figure 2b_1, 2b_3, 2b_5 and the continuous motion is shown in Video M1 from SI). Because of the mobility of electrons on copper, a small mismatch from aligned position would result in severe charge redistribution, resulting in a sharp shaped V_{oc} curve. The experimentally measured V_{oc} is presented in Figure 2d, which has a resembling but slightly different pattern compared to the simulated value in Figure 2c. This is probably due to minor off-alignment during fabrication and measurement, which is discussed in S3 from SI. The FEM simulation also reveals the charge-transferring process between electrodes, as presented in Figure 2e. Induced charges on one electrode exhibit a triangle-shaped pattern with respect to displacement. Again, the experimentally obtained data (Figure 2f) based on a time-integration of the short-circuit current I_{sc} (details presented in S4 from SI) are in good agreement with the simulation result.

To characterize the electric output of the cTENG, I_{sc} and V_{oc} were measured at different sliding velocities. Reciprocating motions were introduced by a velocity-controllable and programmable linear motor, which operated at a stroke of 35 mm. Velocities were programed from 0.3 to 1.0 m/s, with an increment of 0.1 m/s. Accelerations were set at relatively high values to ensure sliding at a uniform velocity within most of the stroke. As shown in Figure 3a, the amplitude of the I_{sc} rises with increasing sliding velocities. Statistical values plotted in Figure 3b exhibit a linear relationship between the current amplitude and the sliding velocities. The maximum value of 668 μA is achieved at a sliding velocity of 1.0 m/s. Such linearity is anticipated because the larger velocity shortens the time (*time* = *l*/*v*, where *l* refers to the sliding distance and *v* the velocity) of a single charge-transport process given that the amount of the transferrable induced charges between electrodes is constant. At the same time, the frequency of the output current is also linearly enhanced. On the other hand, the V_{oc} does not have an apparent dependence on the sliding velocity, as shown in Figure 3c, 3d. In Figure 3c, the V_{oc} densely switched between zero and maximum values, which corresponds to fully aligned and fully displaced positions, staggered. The maximum values only show a minor fluctuation of 110−130 V with a deviation of less than ±8.3%. This is because the V_{oc} is a function of displacement/position instead of the sliding velocity, which is revealed in the simulation results given in Figure 2c.

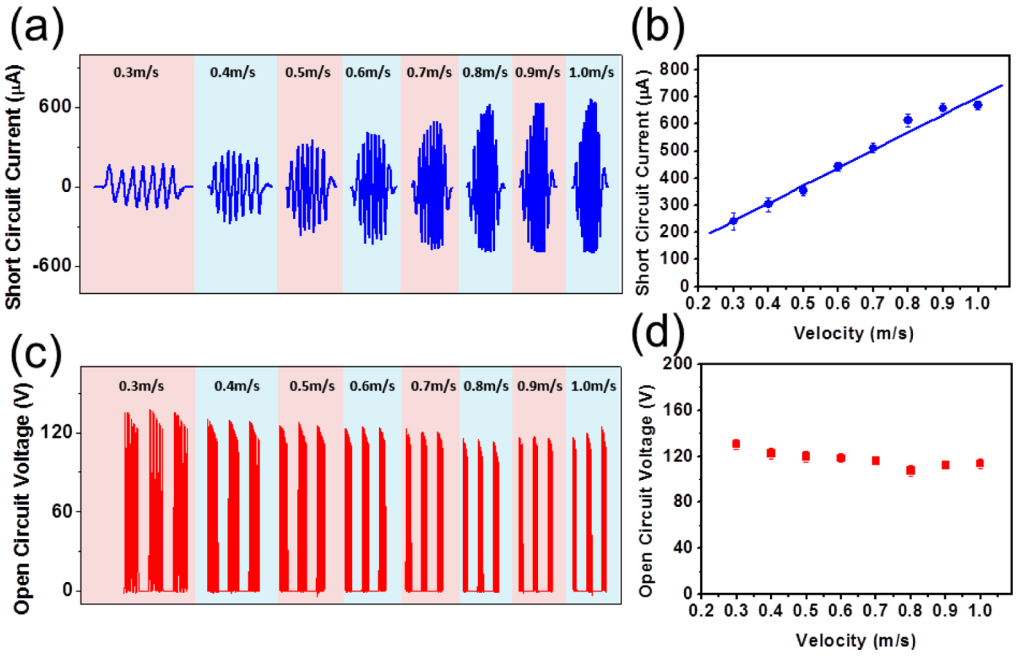

Figure 3. Current and voltage output characters. (a) Short circuit current over different sliding velocities. (b) Current peak values show linear relationship over sliding velocity. (c) Open circuit voltage over different sliding velocities. (d) Voltage peak values do not change much over sliding velocity.

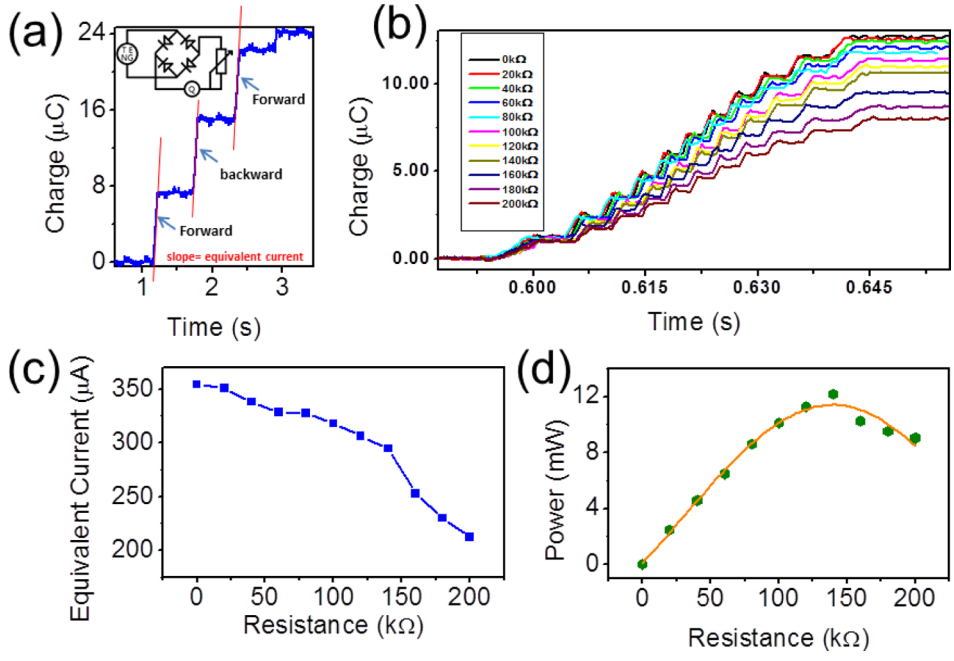

Figure 4. Calculating equivalent current and average power. (a) Measured charge transferred between IE and OE over external load 200 kΩ after rectification at sliding velocity 1 m/s. Slopes of the curve indicate equivalent current. (b) Comparison of charge transfer over different external load. Curves are step-shaped because of the grating electrode. (c) Calculated equivalent current over different external load. (d) Calculated average power over different external load. Peak value of 12.2 mW appears at 140 kΩ.

For further characterization, accumulative induced charges delivered by the cTENG were measured using a bridge rectifier (Figure 4a). A series of load resistors were utilized for output power measurement (Figure 4b, 4c, 4d). A typical curve of the accumulated charges at a load resistance of 200 kΩ is presented in Figure 4a. Each step represents the total amount of output charges generated within a single stroke of sliding at a 1.0 m/s velocity. Consequently, the equivalent current (I_{eq}) in each stroke can be derived by fitting out the slope of a corresponding rising step (see red lines in Figure 4a). With different values of load

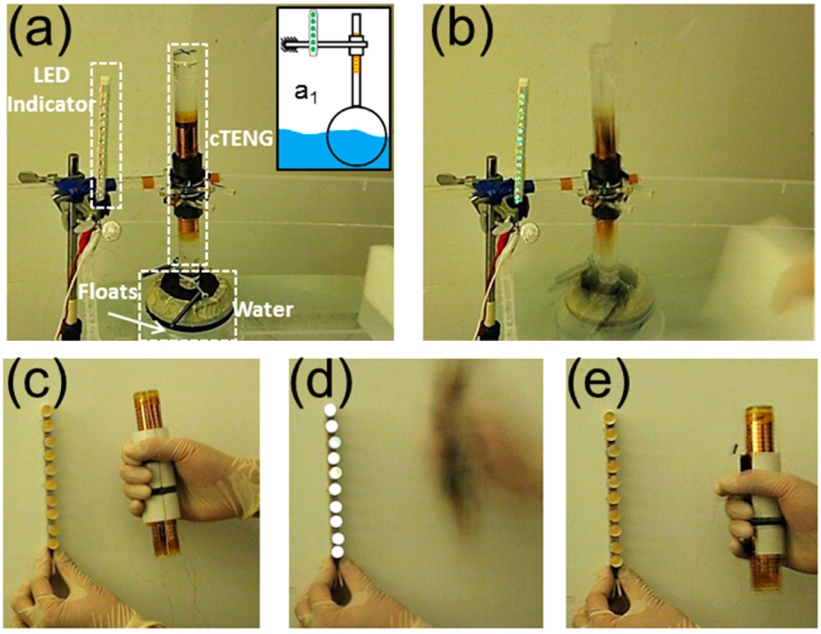

Figure 5. cTENG in application of harvesting reciprocating energy. (a) cTENG was connected to a float to harvest wave energy. Schematic diagram is in (a_1). (b) Green LEDs were lit when artificial wave passed by. cTENG tested in human body motion. White bulbs were driven off–on–off (c) before, (d) during, and (e) after cTENG was shaken by hand.

resistance, the equivalent current varies as shown in Figure 4c, in which larger load corresponds to lower equivalent current. Detailed shape of accumulated charge curve in one complete sliding *via* external load with span from 0 to 200 kΩ was organized into Figure 4b, in which several distinctive features can be observed. With larger external load, the curves end at lower charge levels. For each individual curve, the starting few steps and ending few steps show a smaller slope than the middle ones, meaning they are at lower instantaneous velocity because of the acceleration and deceleration of the linear motor. (One of the signs is the leveled part of the steps from the first and last are longer than the others.) As the slope reflects equivalent current, it is optimal to apply the cTENG on long stroke and large acceleration motions. The obtained equivalent current can be further used to calculate average output power (P_{eq}), which is equivalent to the Joule heating of the external load and, thus, is defined as $P_{eq} = I_{eq}^2 \times R_{load}$. Figure 4d reveals the output power as a function of the external load, which reaches a maximum value of 12.2 mW at a load of 140 kΩ, in corresponding to a power density of 1.36 W/m^2.

To demonstrate the power-generating ability of cTENG, we apply the device to harvest energy from the wave motion of water and human motions. Reciprocating motions, including both periodical (vibration) and nonperiodical forms, widely exist in daily life. Examples include but are not limited to engine cylinders, damping systems, human body motions, and water waves caused by wind, *etc*. In the first demonstration, cTENG was connected to a float and held vertically over the water surface (Figure 5a, 5a$_1$). When wave fronts passed over the float, the fluctuation of the water surface caused float to move up and down, triggering cTENG. Tens of green LEDs powered by the cTENG were lit up (Figure 5b, Video M2 (SI)). Such a demonstration shows potential applications of the cTENG in water (lake/river/marine) navigation fields for self-powered buoy lights, channel lights, underwater obstructions warning lights, *etc*.

The human body motion is another rich source of energy that can be harvested. By simply shaking cTENG, a series of parallel connected white bulbs were lit up (Figure 5c, 5d, 5e, Video M3 (SI)). The cTENG can be further attached to certain parts of the human body, such as hand, forearm, leg or even torso, with its encapsulated casing designed in such a way to permit relative motion in order to generate electricity during human movements due to jogging, jumping, *etc*.

CONCLUSIONS

In summary, we demonstrated a novel style of TENG with an encapsulated cylindrical case that not only delivers a high output but also has several unique features. Grating designed Kapton/copper surface with PTFE particle lubricant ensures a high efficient output. An output current equivalent to a DC source of as high as 0.35 mA and an equivalent power 12.2 mW (corresponding power density 1.36 W/m^2) were achieved during a sliding velocity of 1.0 m/s. The output increases with increasing velocities. Simulations to explain the working mechanism were offered, and detailed features of the charge transfer were studied using FEM. For demonstration, a float-connected cTENG generated enough power to light

up multiple LED bulbs driven by energy of water waves. The cTENG was also applied to harvesting energy from human body motion. This work indicates cTENG as an effective power converter for self-powered electronics.

METHODS

Fabrication of cTENG. Two pieces of Kapton film (25 μm thick) with size 12 cm $\times$ 15 cm (longer one) and 12 cm $\times$ 7.5 cm (shorter one) were prepared and cleaned with isopropyl alcohol. Two pieces of acrylic board (1.5 mm thick) with size 12 cm $\times$ 15 cm (longer one) and 12 cm $\times$ 7.5 cm (shorter one) were prepared by laser cutter. Hollow stripes with individual size 0.2 cm $\times$ 12 cm were brought on such acrylic boards by a laser cutter, arranged parallel in a linear pitch of 4 mm, spread over the available area of two boards. A perpendicular column across all the stripes at their middle point was also engraved. These pierced boards were used as masks for electrode deposition. Kapton films were covered with corresponding-sized acrylic mask on one side and were conducted with copper electrode deposition by physical vapor deposition facilities for the first time. Then same masks were used for the other surface of pretreated Kapton film with a linear shift of 2 mm before conducting with copper deposition. Acrylic cylinder rod with length 15 cm and diameter 3.81 cm was coated with thin layer of polydimethylsiloxane (PDMS) on the surface and was then wrapped with pretreated Kapton film (longer one) as inner part. PTFE particles (DuPont Teflon Non-Stick Dry-Film Lubricant) were spread onto the surface of this Kapton film. The other pretreated Kapton film (shorter one) was then wrapped over (but not stuck to) the inner part, followed by another layer of 0.3 cm thickness double-sided foam tape. Polyethylene terephthalate (PET) film with 75 μm thickness was finally applied onto the outer surface of the foam tape as a support material to complete the casing structure. The outer part was able to move smoothly along the inner part in the manner of piston form. Metal wires were connected to electrode from each surface of the two Kapton films, with electrodes located between contacting surface set as inner electrode (IE), on the back sides of Kapton films set as outer electrode (OE).

Finite Element Analysis Method. Software "Comsol Multiphysics 4.2" was chosen for simulating the open circuit voltage. Model "Electrostatics" was chosen for simulating open-circuit voltage and short-circuit charge transfer. A charge density of 20 μC/m^2 was applied on the Kapton surface as an equivalent result of friction. To reduce the computing complexity, one unit of stripe sliding over 3 units of stripe was simulated. Simulation mainly focused on cross-section and was conducted in 2-dimensional model. To calculate charge, depth of the 2D model was set large enough to meet the actual working area. Width of electrodes and thickness of Kapton were assigned with actual value. Relative permittivity of Kapton was set as 3.4.

Conflict of Interest: The authors declare no competing financial interest.

Acknowledgment. Research was supported by the "thousands talents" program for pioneer researcher and his innovation team, China, Beijing City Committee of science and technology project (Z131100006013004). Chinese Scholarship Council financially supports Qingshen Jing in participating GT-PKU Joint Ph.D. Program during his study in the United States.

Supporting Information Available: (1) Triboelectric series (S1). (2) cTENG behavior influenced by PTFE nanoparticle lubricant (S2). (3) Voltage output affected by improper aligned electrodes (S3). (4) Charge curve calculated from measured current data (S4). (5) Video for voltage output distribution from simulation results (M1). (6) Video of cTENG harvesting energy from wave motion (M2). (7) Video of cTENG harvesting energy from human body motion (M3). This material is available free of charge *via* the Internet at http://pubs.acs.org.

REFERENCES AND NOTES

1. Dresselhaus, M. S.; Thomas, I. L. Alternative Energy Technologies. *Nature* **2001**, *414*, 332–337.
2. Wang, Z. L. Self-Powered Nanosensors and Nanosystems. *Adv. Mater.* **2012**, *24*, 280–285.
3. Wang, X. D.; Song, J. H.; Liu, J.; Wang, Z. L. Direct-Current Nanogenerator Driven by Ultrasonic Waves. *Science* **2007**, *316*, 102–105.
4. Wang, Z. L.; Song, J. H. Piezoelectric Nanogenerators Based on Zinc Oxide Nanowire Arrays. *Science* **2006**, *312*, 242–246.
5. Xu, S.; Qin, Y.; Xu, C.; Wei, Y. G.; Yang, R. S.; Wang, Z. L. Self-Powered Nanowire Devices. *Nat. Nanotechnol.* **2010**, *5*, 366–373.
6. Yang, R. S.; Qin, Y.; Dai, L. M.; Wang, Z. L. Power Generation with Laterally Packaged Piezoelectric Fine Wires. *Nat. Nanotechnol.* **2009**, *4*, 34–39.
7. Mitcheson, P. D.; Miao, P.; Stark, B. H.; Yeatman, E. M.; Holmes, A. S.; Green, T. C. MEMS Electrostatic Micropower Generator for Low Frequency Operation. *Sens. Actuators, A* **2004**, *115*, 523–529.
8. Pelrine, R.; Kornbluh, R.; Eckerle, J.; Jeuck, P.; Oh, S. J.; Pei, Q. B.; Stanford, S. Dielectric Elastomers: Generator Mode Fundamentals and Applications. *Proc. Soc. Photo-Opt. Instrum. Eng.* **2001**, *4329*, 148–156.
9. Arnold, D. P. Review of Microscale Magnetic Power Generation. *IEEE Trans. Magn.* **2007**, *43*, 3940–3951.
10. Williams, C. B.; Shearwood, C.; Harradine, M. A.; Mellor, P. H.; Birch, T. S.; Yates, R. B. Development of an Electromagnetic Micro-generator. *IEE Proceedings, Part G: Circuits, Devices and Systems* **2001**, *148*, 337–342.
11. Chen, J.; Zhu, G.; Yang, W. Q.; Jing, Q. S.; Bai, P.; Yang, Y.; Hou, T. C.; Wang, Z. L. Harmonic-Resonator-Based Triboelectric Nanogenerator as a Sustainable Power Source and a Self-Powered Active Vibration Sensor. *Adv. Mater.* **2013**, *25*, 6094–6099.
12. Zhang, R.; Lin, L.; Jing, Q. S.; Wu, W. Z.; Zhang, Y.; Jiao, Z. X.; Yan, L.; Han, R. P. S.; Wang, Z. L. Nanogenerator as an Active Sensor for Vortex Capture and Ambient Wind-Velocity Detection. *Energy Environ. Sci.* **2012**, *5*, 8528–8533.
13. Hu, Y. F.; Xu, C.; Zhang, Y.; Lin, L.; Snyder, R. L.; Wang, Z. L. A Nanogenerator for Energy Harvesting from a Rotating Tire and its Application as a Self-Powered Pressure/Speed Sensor. *Adv. Mater.* **2011**, *23*, 4068–4071.
14. Lee, M.; Chen, C. Y.; Wang, S.; Cha, S. N.; Park, Y. J.; Kim, J. M.; Chou, L. J.; Wang, Z. L. A Hybrid Piezoelectric Structure for Wearable Nanogenerators. *Adv. Mater.* **2012**, *24*, 1759–1764.
15. Lee, M.; Bae, J.; Lee, J.; Lee, C. S.; Hong, S.; Wang, Z. L. Self-Powered Environmental Sensor System Driven by Nanogenerators. *Energy Environ. Sci.* **2011**, *4*, 3359–3363.
16. Fan, F. R.; Lin, L.; Zhu, G.; Wu, W. Z.; Zhang, R.; Wang, Z. L. Transparent Triboelectric Nanogenerators and Self-Powered Pressure Sensors Based on Micropatterned Plastic Films. *Nano Lett.* **2012**, *12*, 3109–3114.
17. Wang, S. H.; Lin, L.; Wang, Z. L. Nanoscale Triboelectric-Effect-Enabled Energy Conversion for Sustainably Powering Portable Electronics. *Nano Lett.* **2012**, *12*, 6339–6346.
18. Yang, Y.; Lin, L.; Zhang, Y.; Jing, Q. S.; Hou, T. C.; Wang, Z. L. Self-Powered Magnetic Sensor Based on a Triboelectric Nanogenerator. *ACS Nano* **2012**, *6*, 10378–10383.
19. Wang, Z. L. Triboelectric Nanogenerators as New Energy Technology for Self-Powered Systems and as Active Mechanical and Chemical Sensors. *ACS Nano* **2013**, *7*, 9533–9557.
20. Leland, E. S.; Wright, P. K. Resonance Tuning of Piezoelectric Vibration Energy Scavenging Generators Using Compressive Axial Preload. *Smart Mater. Struct.* **2006**, *15*, 1413–1420.

21. Challa, V. R.; Prasad, M. G.; Shi, Y.; Fisher, F. T. A Vibration Energy Harvesting Device with Bidirectional Resonance Frequency Tunability. *Smart Mater. Struct.* **2008**, *17*, 015035.
22. Beeby, S. P.; Torah, R. N.; Tudor, M. J.; Glynne-Jones, P.; O'Donnell, T.; Saha, C. R.; Roy, S. A Micro Electromagnetic Generator for Vibration Energy Harvesting. *J. Micromech. Microeng.* **2007**, *17*, 1257–1265.
23. Hu, Y. F.; Yang, J.; Jing, Q. S.; Niu, S. M.; Wu, W. Z.; Wang, Z. L. Triboelectric Nanogenerator Built on Suspended 3D Spiral Structure as Vibration and Positioning Sensor and Wave Energy Harvester. *ACS Nano* **2013**, *7*, 10424–10432.
24. Wang, S. H.; Lin, L.; Xie, Y. N.; Jing, Q. S.; Niu, S. M.; Wang, Z. L. Sliding-Triboelectric Nanogenerators Based on In-Plane Charge-Separation Mechanism. *Nano Lett.* **2013**, *13*, 2226–2233.
25. Zhu, G.; Chen, J.; Liu, Y.; Bai, P.; Zhou, Y. S.; Jing, Q. S.; Pan, C. F.; Wang, Z. L. Linear-Grating Triboelectric Generator Based on Sliding Electrification. *Nano Lett.* **2013**, *13*, 2282–2289.